Full length article

Angle-dependent reflectance measurements on photovoltaic materials and solar cells

Antonio Parretta [a,*], Angelo Sarno [a], Pierpasquale Tortora [a], Haruna Yakubu [a,1], Pasqualino Maddalena [b], Jianhua Zhao [c], Aihua Wang [c]

[a] *ENEA Centro Ricerche, Località Granatello, C.P. 32, I-80055 Portici (Na), Italy*
[b] *INFM, Dipartimento di Scienze Fisiche, Università di Napoli 'Federico II', Monte S. Angelo, Naples, Italy*
[c] *Photovoltaics Special Research Centre, University of New South Wales, Sydney, NSW 2052, Australia*

Abstract

Results of angle-dependent reflectance measurements on photovoltaic materials and solar cells are presented and discussed. The optical apparatus employs an integrating sphere of 40 cm diameter and it is suitable for working at variable wavelengths and incidence angles of the light beam. Directional/hemispherical reflectance measurements can be performed and both the diffuse and the total components of the reflected light can be obtained. Samples of any size can be measured by this apparatus, including small prototype solar cells (≤ 2 cm), medium size materials and solar cells (10–12 cm), as well as glass sheets and entire photovoltaic modules. Results of reflectance on silicon materials, commercial and record efficient silicon solar cells are here presented as functions of the incidence angle and wavelength of the light beam. The measurements evidence the superior light trapping performances of the inverted pyramids (PERL) and of the new 'honeycomb' structures with respect to the traditional upright random pyramids texturization. A simple analytical model describing the effect of the grid is derived and discussed. The model was used to calculate the reflectance of the exposed semiconductor region of the cell only. It was validated by comparing the calculated reflectance of the semiconductor region with that measured on 'gridless' cells. The spectral reflectance measurements at different angles matched the light collection performances of the cells, and are very useful for their optimization in view of their outdoor application. © 1999 Published by Elsevier Science B.V. All rights reserved.

1. Introduction

---
* Corresponding author. Tel.: +39-081-7723262; fax: +39-081-7723344; e-mail: parretta@epocal.portici.enea.it
[1] Permanent address: Department of Physics, University of Cape Coast, Cape Coast, Ghana.

The knowledge of the reflectance of a photovoltaic (PV) device is important to derive its internal spectral response, its absolute optical loss and, particularly for an encapsulated cell or a PV module in

outdoor operation, its optical loss relative to the standard test conditions (STC) [1,2]. Measuring the reflectance at different incidence angles and wavelengths allows to know, and then to improve upon, the light collection capabilities of the PV device respect to the direct component of the sunlight or to the diffuse radiation from the sky hemisphere [2].

PV devices or materials are usually characterized by the spectrophotometer method. That method generally requires small samples and operates at a fixed incidence angle ($\theta = 8°$). The method presented in this paper has the advantage to allow the characterization of both small and large samples (PV modules, large glass sheets, etc.), and to operate at variable incidence angles of the light beam. It is based on the use of an apparatus (reflectometer) which is described here only relatively to the characterization of small samples. Details on its application to the characterization of PV modules or large glass sheets can be found elsewhere [3–5]. The light collection properties of unencapsulated screen printed and record efficient c-Si cells are compared. The influence of the grid on the reflectance measurements is taken into account. An analytic model describing the grid effect has been applied and verified.

2. Experimental

2.1. Description of the optical apparatus

The variable angle reflectometer [3–5], also called ROSE (reflectometer for optical measurements in solar energy) due to its versatility and usefulness in the characterization of solar energy materials and PV devices, was built by MACAM Photometrics. It consists of three major parts: an integrating sphere, a light source and a radiation detection system. The integrating sphere collects all the light reflected by the sample and measures the respective total reflectance. The sphere also measures the diffuse reflectance when the specularly reflected beam is selectively absorbed by a light trap. The integrating sphere, 40 cm in diameter, was fitted with a number of ports. For reflectance measurements on small PV samples (see Fig. 1) the sample (c) was mounted on the sample holder (p), inserted into the sphere through a port placed on top of it. The sphere was fitted, on its equatorial line, with ports for the input of the light beam and other ports for the output of the specularly reflected beam. Specular ports were arranged from 10° to 70° angles in steps of 10°. The light source (l), which was a laser or a lamp (QTH, Xenon, etc.), was
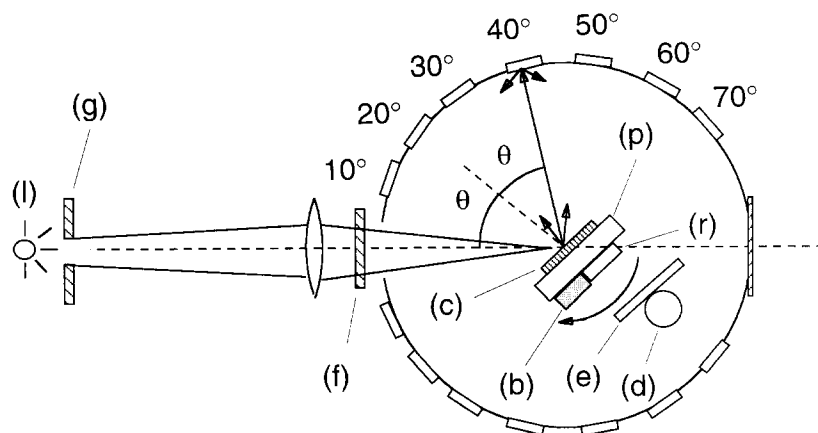

Fig. 1. Schematic diagram of the top view of the ROSE apparatus in the configuration for filter spectral reflectance measurements on small sample. The sample is placed at the center of the sphere. All the ports, except 0° for the input of light, are closed. A 40° total reflectance measurement is illustrated.

directed towards the 0° port. The head of the sample holder (p) was rotated to change the incidence angle to the sample. Using a laser and a sample of about 2 cm in size, incidence angles as high as $\approx 85°$ could be reached. Incidence angles of $\theta \approx 70–80°$ could be reached by using a lamp light focused on the sample.

The irradiance into the sphere was measured by a silicon photodiode (d) which was facing one port located at the bottom of the sphere and protected by a baffle (e) from direct reflections from the sample. Filter spectral measurements were performed by mounting a filter (f) between the light source and the input port of the sphere (see Fig. 1).

2.2. Samples

The characterized samples were silicon materials and solar cells. They were: mono-Si samples of different surface treatments, screen printed monocrystalline silicon (c-Si) solar cells from Eurosolare (ES), c-Si PERL (passivated emitter, rear locally-diffused) cells and multicrystalline silicon (m-Si) honeycomb (HC) solar cells from UNSW [6–8], and an encapsulated c-Si solar cell (EC) used as reference to investigate the effect of the glass sheet. The Si + ARC sample was a Si wafer with a TiO_2/SiO_2 (450/950 Å) coating. The text, Si + ARC sample was a Si wafer, textured with upright pyramids, and coated by a TiO_2 (400 Å) layer.

The PERL cells and HC cells have demonstrated energy conversion efficiencies of 24.4% and 19.8%, respectively, which are the highest ever reported efficiencies for c-Si and m-Si solar cells [7,8]. The ES cells were fabricated with randomly textured upright pyramids (5–10 μm size), screen printed silver front grid, and coated with a TiO_2 antireflection coating (ARC). The front finger spacing was ≈ 3 mm, the fingers width was ≈ 140 μm and the fingers height was ≈ 12 μm. The structure of the PERL cell is shown in Fig. 2(a) and Fig. 2(b). These PERL cells were fabricated on a Wacker bright etched FZ c-Si substrate (450 μm thick) with front texturing of 10 μm-sized inverted pyramids, and coated with a double-layer antireflection coating of ZnS/MgF_2 of thickness 350/1100 Å on a passivation silicon dioxide of 200 Å thickness [6]. Their front grid was electrically plated silver, also covered by the ZnS/MgF_2 double layer. The spacing be-

tween fingers was 800 μm. The rear surface was SiO_2 (5000 Å) covered by a thick layer of aluminium. The HC cells (see Fig. 3(a) and Fig. 3(b)) were fabricated on a m-Si substrate from Eurosolare (260 μm thick). Their front surface was textured with a honeycomb structure of hemispherical wells of 14 μm spacing, hexagonally placed on the surface [8]. These HC cells had the same front antireflection coating and passivation oxide structure and the same metal finger pattern as the PERL cells. They had also the same rear surface structure as the PERL cells. Some 'gridless' PERL and HC cells (gl-PERL and gl-HC) test samples were also fabricated with standard inverted pyramids and honeycomb structures covering the entire front surface of a Wacker bright etched FZ substrate and a Eurosolare's m-Si substrate, respectively. A standard ZnS/MgF_2 double layer antireflection coating was also deposited on these test samples. The grid of the PERL and HC cells could not be chemically etched being covered by the ARC, while this was easy done with the grid of the ES cells which were made of just silver.

2.3. Optical measurements

The light sources used for the reflectance measurements were an unpolarized 20-mW Oriel He–Ne laser of $\lambda = 633$ nm and a stabilized 250 W Oriel QTH lamp. Whenever possible, the laser beam was directed onto regions between two adjacent fingers of the tested cell, in order to measure only the reflectance from the semiconductor area of the device - the optically active (oa) area. For this purpose, the cells were oriented (azimuth angle) with the fingers parallel to the incident plane of the beam. In this way, the laser beam remained focused between the two fingers at the different incidence angles, avoiding the grid effects. The 800 μm finger spacing in the PERL and HC cells was too small compared with the diameter of the laser beam of about 1.5 mm. Hence, some portions of the fingers were always illuminated by the laser beam, contributing to the reflectance of these cells. The spectral reflectance measurements at variable incidence angles taken by ROSE were carried out at light levels in the order of ≈ 1 mW/cm^2, using the QTH source and filters of 70 nm bandwidth (see Fig. 1). The calibration of ROSE for the reflectance measurements was accom-

plished in two ways: (i) by a preliminary measurement of the spectral reflectance on each sample by a Perkin Elmer Lambda 9 spectrophotometer (SP) with an incidence angle of $\theta = 8°$; and (ii) by using a standard of reflectance (r) ($R \approx 100\%$) and a black absorber (b) ($R \approx 0\%$), both mounted on the sample holder (p) on the opposite side of the sample (see Fig. 1). Both the standard and the absorber were
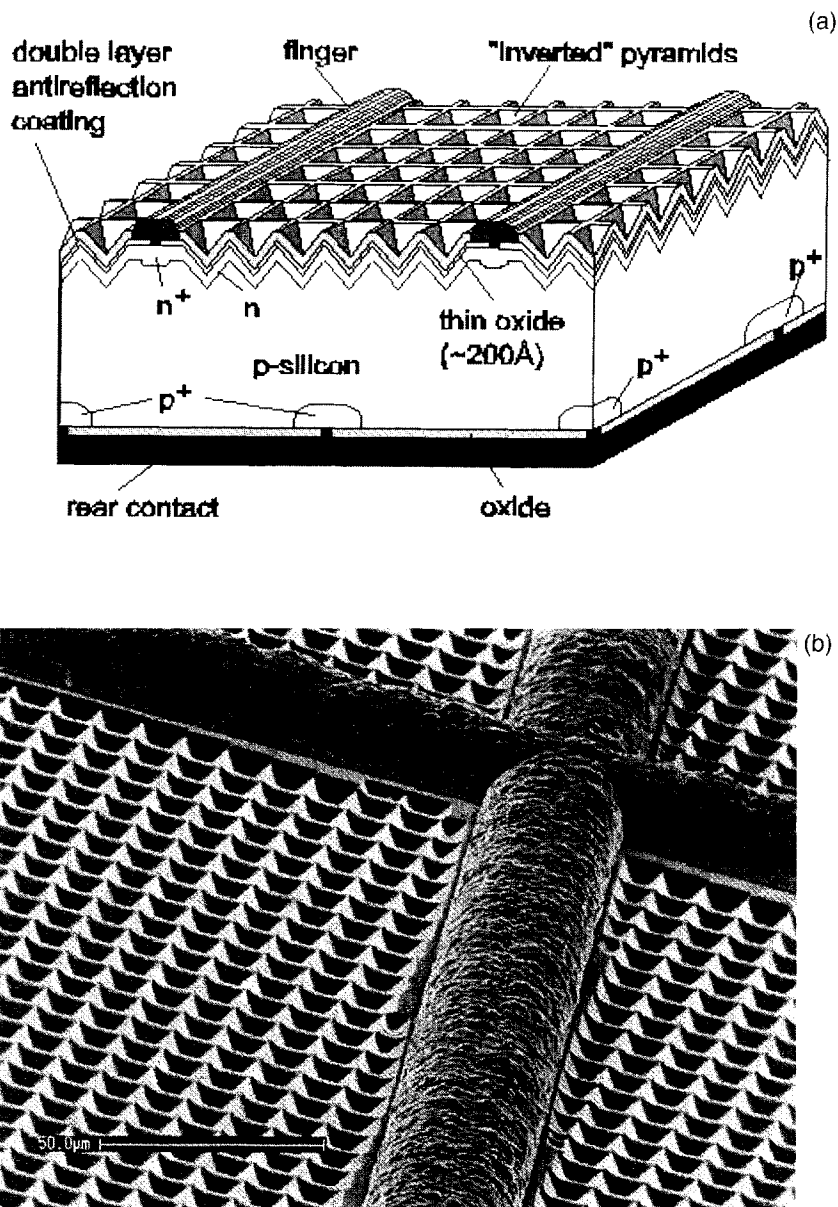

Fig. 2. (a) The structure of the PERL cell. The cell front surface, processed by photolithography, is textured with regular pyramids. In the figure, the pyramids have bases parallel to the fingers. (b) SEM picture of the PERL cell surface, with the semi-circularly shaped fingers and the inverted pyramids. The pyramids form an array which is slightly inclined with respect to the fingers. The segment in the figure is equivalent to 50 μm.

measured in the sphere just before and after any series of reflectance measurements. The sample itself could also be used as the reference at 8°, because it was already calibrated by the SP. However, this was
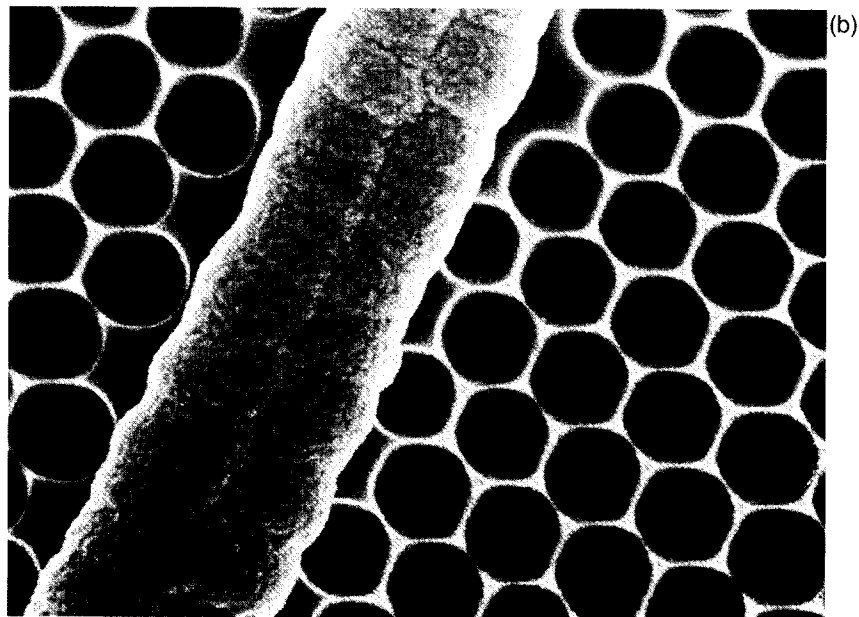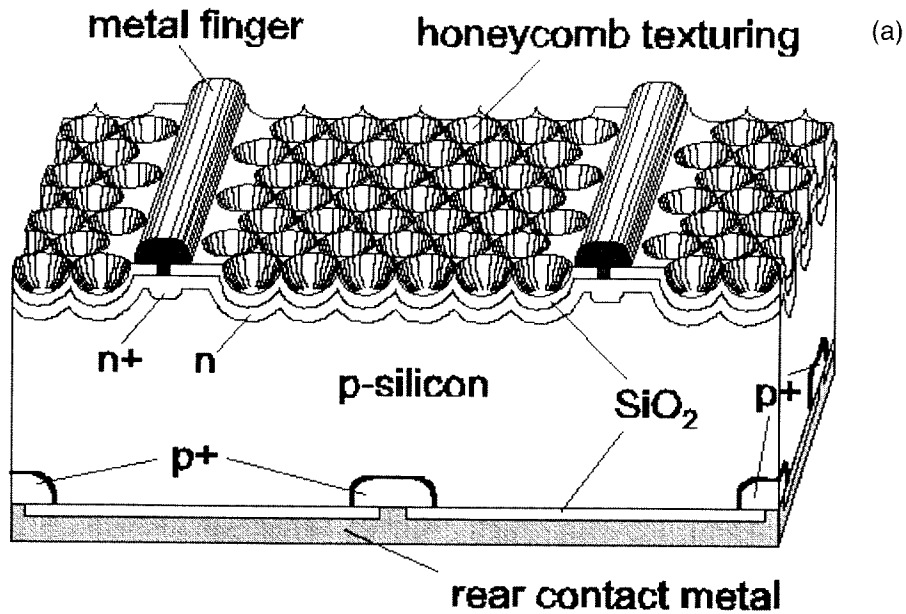

Fig. 3. (a) The structure of the 'honeycomb' (HC) cell. The HC cells have a surface structure consisting of hexagonally placed hemispherical 'wells'. They were processed similarly to the PERL cells, except for their thinner multicrystalline substrate and for the surface texturization. (b) SEM picture of the HC cell surface, with the hemispherical wells. The fingers are similar to those of the PERL cells.

not always possible since it may be very difficult to select the same area in the two measurements for SP and ROSE. In general, the accurate selection of the sample area is a difficult task for the SP, which uses a fixed area of about 1 cm^2 of the port for the sample. This area always comprises some grid when a solar cell is measured. On the contrary, the ROSE allows a better selection of the sample area for the measurement, at least by the limit of the light beam dimension, also thanks to the flexibility of the light source and to the particular configuration and volume of the sphere. The ROSE allows a further control to the illumination area, due to the use of a viewport on top of the sphere.

3. Modeling of the grid effect

The need for modeling the influence of the grid on the optical properties of a solar cell comes from different reasons. The optical reflectance measurements on the cell are aimed at knowing the optical loss from the optically active region of the cell, $R_{oa}(\theta)$, in order to improve upon the light trapping and collection capabilities of the cell, and hence its efficiency. In this respect, the reflectance of the grid is a disturbance in the measurements and should be avoided. One way to do this is to fabricate a 'gridless' cell, specially designed for the optical measurements. Another way is to build an analytic model for the grid reflectance and to subtract its effect from the measurement result of a true cell. In the following, the reflectance of the optically active region, $R_{oa}(\theta)$, is calculated based on the measurements from the true cell, $\underline{R}(\theta)$. This simple proposed model has been verified for the unencapsulated cells. It can be applied, therefore, to any newly designed device, avoiding in this way the fabrication of the 'gridless' samples.

When the light spot on the cell surface is larger than the spacing between two adjacent fingers, the measured reflectance is a combined effect of that from the optically active (oa) area (Silicon + ARC) and of that from the metal grid (see Fig. 4(a)). Although the grid area is only a few percent of the total cell area, its high reflectivity ($\geq 90\%$ for silver, a common grid metal for Si cells) significantly increases the average reflectance of the illuminated
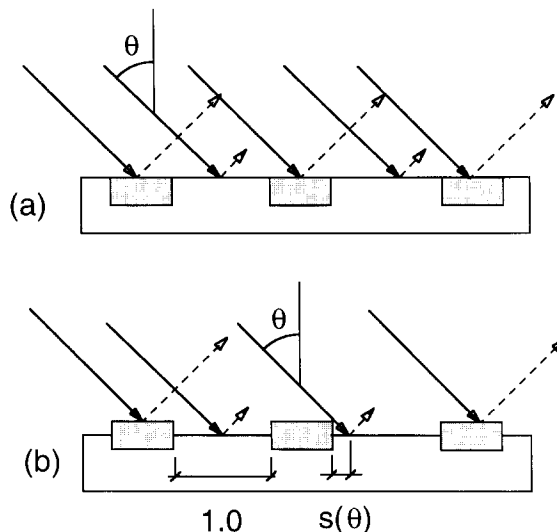

Fig. 4. Diagrams showing the simplified surface of an unencapsulated solar cell: (a) the light is reflected by the surface from the fingers and from the 'optically active' area of the semiconductor; and (b) in a real unencapsulated cell, the fingers protrude above the cell surface and produce a shadowing effect over the active area.

cell area. To obtain the reflectance of the oa region alone, some corrective formulae have to be applied. Neglecting the dependence on ϕ (the azimuth angle of the light incident plane) when the cell is anisotropically textured, the reflectance of the oa region can be expressed as:

$$R_{oa}(\theta) = \left[\underline{R}(\theta) - R_g(\theta)S_g\right]/(1 - S_g) \qquad (1)$$

where θ is the incidence angle of the light beam, $R(\theta)$ is the measured reflectance, $R_g(\theta)$ is the grid reflectance and S_g is the grid fraction area.

S_g, if not known, can be measured by an optical microscope. $\underline{R}(\theta)$ is obtained with the spot of light illuminating only the finger region of the cell (not the busbar). For integrated a-Si or CIS cells, a single measurement between two adjacent laser scribed lines is sufficient to obtain $R_{oa}(\theta)$. If the absorbance of the window layers, $A_{oa}(\theta)$, is known, the absolute 'transmittance' of the oa area, $T_{oa}(\theta)$, can be expressed as:

$$T_{oa}(\theta) = \left[1 - \underline{R}(\theta) - S_g\left[1 - R_g(0°)\right]\right.$$
$$\left. - (1 - S_g)A_{oa}(\theta)\right]/\left[1 - S_g\right]. \qquad (2)$$

We introduce the 'relative transmittance', $\tau(\theta)$, of the cell with respect to the normal incidence [5]:

$$\tau(\theta) = T_{oa}(\theta)/T_{oa}(0°)$$
$$= [1 - R_{oa}(\theta)]/[1 - R_{oa}(0°)] \qquad (3)$$

$\tau(\theta)$ is a useful parameter in the description of the light collection properties of a solar cell, particularly when considering the incident light in real operating conditions. For an unencapsulated cell, the quantity $A_{oa}(\theta)$ in Eq. (4) can be neglected since it reduces to the absorbance of the thin antireflection coating. When the finger is protruding above the cell plane (see Fig. 4(b)), a shadowing effect is produced over the active area and Eq. (1) must be slightly modified. If $s(\theta)$, named the 'shadowing factor', is the fraction of active area shadowed by the finger, we have:

$$R_{oa}(\theta) \approx \left\{ \underline{R}(\theta) - S_g\left[1 + s(\theta)/S_g\right] R_g(\theta) \right\}$$
$$/ \left\{ [1 - s(\theta)](1 - S_g) \right\} \qquad (4)$$

where the fraction area, S_g, corresponds to the base of the finger.

4. Experimental results and discussion

4.1. Reflectance measurements at $\lambda = 633$ nm

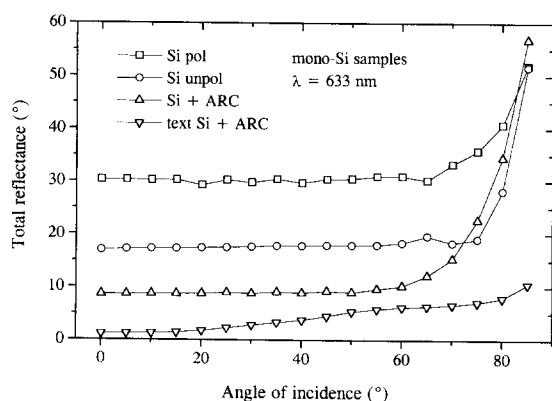Fig. 5 shows the curves of total reflectance, $R_{tot}(\theta)$, of some silicon materials as a function of the

Fig. 5. Total reflectance, $R_{tot}(\theta)$, of mono-silicon samples with different surface treatments. The reflectance is shown as a function of the incidence angle of a 1 mW He–Ne laser beam of $\lambda = 633$ nm. The irradiance at $\theta = 0°$ was about 50 mW/cm^2. The textured and ARC coated silicon shows the lowest reflectance even at the highest angles.

incidence angle of the laser beam. The values of reflectance at near normal incidence for these materials are well known, as they are commonly obtained by measurements on commercial spectrophotometers. The polished silicon surface shows the highest reflectance values. It is followed by the unpolished silicon, whose rough surface favours the collection of light. A planar silicon surface with an antireflection coating shows a further lower reflectance. The lowest reflectance is finally obtained with textured silicon with random upright pyramids, covered with an ARC layer, due to the so-called double bounce effect [9]. At varying the incidence angle of the light beam, we find that all the curves, except that of the textured wafer, keep flat up to 60–70°, after which a sharp increase of reflectance is observed. A completely different behaviour is observed for the textured silicon sample. The reflectance has a minimum at near $\theta = 0°$, since the double bounce effect is most effective under the low incidence angles, and slightly increases remaining below 10% even at the highest angles. The difference found on the reflectance between a planar and a textured silicon wafer is relevant over the entire range of angles. This is a well established result which explains the necessity of texturing the silicon surface to reduce the optical loss of the cell and hence to increase its efficiency.

Fig. 6 shows the total reflectance curves of all the tested cells as obtained by ROSE, at $\lambda = 633$ nm, by varying the incidence angle θ. These measurements were taken by orienting the cells with their grid fingers parallel to the incident plane of the laser beam ($\phi = 0°$) while trying to keep the laser beam focused between two fingers. As discussed in the experimental section, this was to minimize the disturbance of the grid on the measurements. Due to the large finger spacing (> 2.5 mm) for the ES and EC cells, the laser beam illuminated only the active area of these cells in the measurement, and the measured reflectance was that of the oa region, $R_{oa}(\theta)$. Due to the small finger spacing of only 800 μm for the PERL and HC cells, on the contrary, the laser beam illuminated both the optically active area and the finger area. Hence, the measured reflectance was a combined contribution from both areas. In spite of the presence of the grid, the reflectance of the PERL cell is very low (about 2% at low angles) and keeps constant up to about 80°. This low reflectance is a
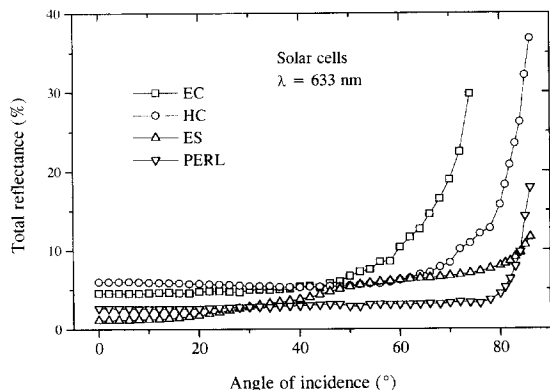
Fig. 6. Curves of total reflectance, $R_{tot}(\theta)$, of four types of tested solar cells, as a function of the incidence angle of the laser beam. The irradiance on the sample was about 1 W/cm², at $\theta = 0°$. All the textured cells show superior optical properties. The PERL cell, in particular, shows the lowest reflection, that maintains up to an angle as high as 80°.

result from the excellent light collection performances of the inverted pyramids structure. With this structure, an incident beam at low angles strikes the cell surface twice before being reflected away from the cell and thus has two chances of being absorbed (see Fig. 7). At high incidence angles, the light strikes the (111) facets of the pyramids almost orthogonally (see Fig. 7). This condition favours the transmission of light into the semiconductor. Also the ES cell shows low reflectance values because of the presence of similar geometrical structures (upright pyramids). However, a different behaviour is found between the two curves of Fig. 6, at increasing angles, which may have come from the different orientation of the pyramids in the two cells with respect to the fingers direction. The inverted pyramids, in fact, have their bases aligned to the finger direction, whereas the upright pyramids have their bases aligned in a 45° angle to the fingers. Also, the flat bases of the inverted pyramids may have further reduced the large angle reflectance than the sharp peaks of the upright pyramids. A detailed theoretical discussion about the light trapping performances of the inverted pyramids structure, as well as of other texturing schemes, can be found in Ref. [10]. The HC cells, with their honeycomb design, have been realized only recently and the reported reflectance values, here, are a novelty. A description of their optical properties is also reported by Green et al.

[11]. At increasing incidence angles, our tested HC cell shows a slight decrease of the reflectance with a minimum at around 40° and a sharp increase after 70°. The collection of light at high angles is markedly different respect to the PERL cell. This fact can be attributed to the crossing, by the light rays, of the intersecting regions between two neighbouring wells, with a consequent decoupling of a fraction of light from the cell. This point will be better discussed later in this section. The EC cell shows a reflectance curve which bends upwards just after 40°. The EC cell reflectance is strongly conditioned by the presence of the glass cover sheet. In this regard, trying to find a simple model for the optical reflectance of a PV module, we have recently observed [5] that, as far as the transmittance of the module relative to the normal incidence, $\tau(\theta)$, is concerned (see Eq. (3)), the module behaves like a homogeneous, semi-infinite, dielectric of equivalent refractive index, n_{eq}, higher than that of glass ($n = 1.5$) and dependent on the particular structure of the layers below the glass/EVA/glass cover sheet. The study on commercial PV modules resulted in n_{eq} values which mostly fall in the 2.5–3.0 range. The EC encapsulated cell should behave similarly to a PV module, due to the presence of glass in front of it. We have compared, therefore, the relative transmittance curve, $\tau(\theta)$, of the EC cell with that calculated for dielectrics of different refractive indices, and found that the theoretical curve relative to a refractive index of $n = 2.0$ is that which better matches the experimental curve of the EC cell (see Fig. 8). With respect to the relative transmittance, therefore, the EC cell behaves like a homogeneous, semi-infinite, dielectric with an equivalent refractive index $n_{eq} \approx 2$.
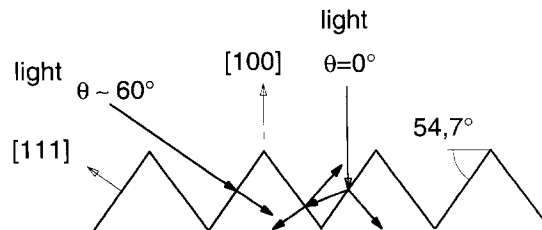

Fig. 7. Schematics of the geometric optics describing the reflection of a light beam on the surface of a silicon sample textured by regular pyramids. Both low and high angles of incidence are favoured by this type of surface texturization.
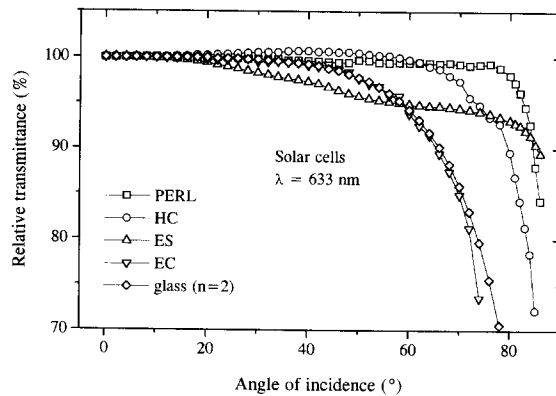
Fig. 8. Transmittance of the tested cells, at $\lambda = 633$ nm, normalized to that at normal incidence, $\tau(\theta) \approx [1 - R_{tot}(\theta)]/[1 - R_{tot}(0°)]$. The PERL cell has superior optical transmittance properties, but the HC (honeycomb) cell shows an interesting high relative transmittance at angles $\theta \leq 60°$. The EC cell is compared to the theoretical transmittance curve of a dielectric with refractive index $n = 2$. The EC cell behaves like a homogeneous dielectric of equivalent refractive index $n_{eq} = 2$.

The value found for n_{eq}, lower than expected, could depend on differences between the glass used in the EC cell and the special glass used in a PV module [12]. Even though not showing the lowest reflectance (see Fig. 6), the HC cell gives the highest relative transmittance at intermediate angles (see Fig. 8), as its reflectance shows a slight decreasing behaviour in this range. This may be a result from the hemispherical shape of the wells and, in particular, from the presence of flat regions near the wells bottom [11].

To derive the reflectance only from the active region of the tested cells, $R_{oa}(\theta)$, the contribution from the grid can be extracted by applying the method described in Section 3. To obtain the $R_{oa}(\theta)$ curves of the PERL and HC cells, the reflectance of silver grid coated with the ZnS/MgF$_2$ double layer should be known, as stated by (1). To avoid its calculation, which is complicated by the fact that the grid surface is neither simply metal nor flat, the grid was removed from the cells and the underlying silicon exposed. The reflectance of the cells was measured again (see Fig. 9 for the PERL cell) and corrected for the presence of flat 'silicon finger' regions by utilizing the experimental values of reflectance measured from polished silicon wafers (see Fig. 5). Fig. 9 shows how the original reflectance curve (a) of the PERL cell is modified after the

removal of the grid (b) and after the correction for taking into account the silicon reflectance (c). To confirm the procedure used for the calculation of $R_{oa}(\theta)$, a special sample was fabricated without the grid or the flat grid regions (they are indicated with the prefix 'gl'), and its reflectance was also measured as curve (d). Comparing the calculated (c) and measured (d) reflectance curves of the optically active area of the PERL cell as shown in Fig. 9, it is found that they overlap fairly well up to 75°. The deviation of the curves at higher angles may be a result from the processing difference of the two samples. After this result, the method presented in Section 3 can be considered validated when applied to unencapsulated cells. The 'bumps' on the reflectance curves at about 50° and 75° are instrumental effects due to the absorbance of some reflected spots by dark areas inside the sphere.

The reflectance of anisotropic cells depends on, besides the incidence angle θ, also on the azimuth angle, ϕ, that one which the incident plane of the light makes with an arbitrary plane orthogonal to the cell surface, taken as reference. Not being textured, the EC cells are isotropic with respect to the plane of the cell. Therefore, their $R_{oa}(\theta)$ curve is independent of the azimuth orientation of the laser beam, ϕ. The
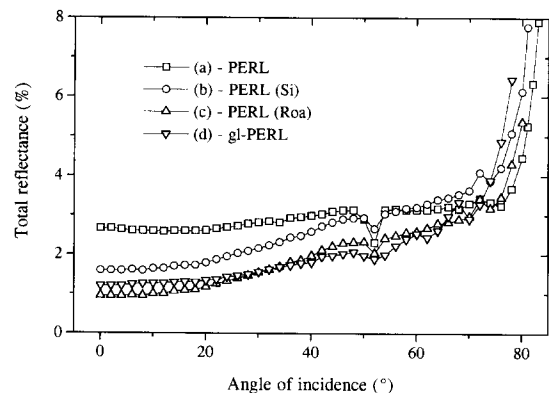

Fig. 9. Experimental and theoretical total reflectance, $R_{tot}(\theta)$, at $\lambda = 633$ nm, of the PERL cell after different surface treatments: (a) normal PERL cell; (b) PERL cell after the removal of the grid, exposing the underlying silicon; (c) correction of the (b) curve for subtracting the reflectance of silicon; and (d) measured reflectance of the special 'gridless' cell, equivalent to a standard PERL cell without grid. The agreement between curves (c) and (d) confirms that the calculation method used for taking into account the grid reflectance is acceptable.
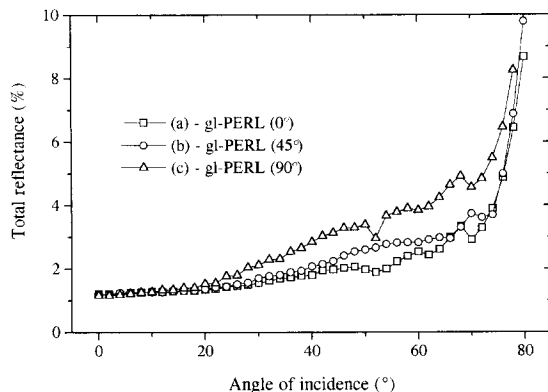
148   A. Parretta et al. / Optics Communications 172 (1999) 139–151

Fig. 10. Total reflectance, $R_{tot}(\theta)$, at $\lambda = 633$ nm, of the 'grid-less' PERL cell at different azimuth angles of the incident laser beam. The difference between $\phi = 0°$ and $\phi = 90°$ is attributed to nonsymmetrical photolitography and wet etching process.

same should happen for the HC cells, since their surface is hexagonally structured and each well has a roughly hemispherical shape (see Fig. 3(b)). Due to the presence of the pyramids, the ES and PERL cells should show an anisotropic behaviour with respect to the light orientation. Therefore, a complete analysis of their optical properties and a correct comparison between them and the isotropic cells should require the measurements of the reflectance at different values of their azimuth orientation, at least in an interval of 90°. The 'gridless' PERL cell, gl-PERL, was characterized at different azimuth angles at $\lambda = 633$ nm. The results are reported in Fig. 10. All the shown curves converge at $\theta = 0°$, as it was expected, since at this incidence angle the azimuth orientation of a structured cell is unimportant when the light is unpolarized. The curve at $\phi = 0°$ corresponds to a cell with the fingers oriented parallel to the light incident plane and shows the lowest reflectance values. A rotation of 45° in azimuth gives a slightly higher reflectance at θ angles different from 0°. The curve at $\phi = 90°$ corresponds to a cell with the fingers oriented orthogonal to the light incident plane. Due to the 90° symmetry of the pyramids, the $\phi = 0°$ and $\phi = 90°$ curves were expected to overlap. However, this does not always happen, since the inverted pyramids sometimes have different x and y widths of flat areas. This is a result from nonsymmetrical photolitography and wet etching process. This finally results in a slightly different optical performance

along x and y directions on the cell plane. No matter what, the inverted pyramid cells gave a considerably lower reflection at $\phi = 45°$ than the random upright pyramids structure as seen in Fig. 6. These experimental results confirm the advantages of the inverted pyramids over upright pyramids and their superior reflectance properties at high angles of incidence, as already deduced by theoretical investigations [10,13].

4.2. Spectral reflectance measurements

All the cells were also tested under different wavelengths of the incident light with the system scheme shown in Fig. 1. The light irradiance on the sample, at $\theta = 0°$, was about 1 mW/cm^2 at all the wavelengths. The irradiance, of course, was dependent on the incidence angle, θ, and reduced by a factor $1/\cos(\theta)$ at increased θ. Therefore, the spectral reflectance curves presented afterwards will depend, in principle, not only on the angle of incidence, θ, but also on the irradiance. Even if a study on the optical reflectance of these cells as a function of the irradiance level was not yet completed, we believe that the irradiance, being so low even at 0°, should not have affected the measurement results.

Fig. 11 shows the spectral reflectance of the gl-PERL cell at different incidence angles. The gl-PERL cell was measured at the azimuth of $\phi = 0°$. This orientation corresponds to that with the fingers parallel to the incident plane of the laser light beam. The reflectance curves in Fig. 11 change significantly at different θ. In particular, the shortest and longest wavelengths are more reflected at high incidence angles (a threefold and fivefold increase of reflectance is observed, respectively). On the intermediate portion of the spectrum, only a twofold increase of reflectance is observed. The minimum of the reflectance curves slightly shifts from 800 nm to 700 nm, as an effect of the different spectral reflectance of the ARC when the light rays, in their multiple bounces on the pyramid facets, change their angles of incidence respect to it. A similar effect was observed on the same ZnS/MgF$_2$ ARC structure by varying the thickness of the two layers [14]. In conclusion, the cell, when inclined, maintains its light collection capabilities optimized respect to the medium wavelengths range, and these can be consid-
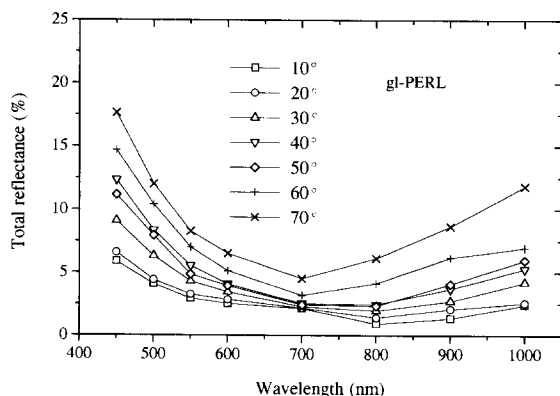
Fig. 11. Filter spectral reflectance, $R_{tot}(\theta,\lambda)$, of the 'gridless' PERL cell, reported at different incidence angles of a QTH lamp light beam. The irradiance at $\theta = 0°$ incidence was about 1 mW/cm^2. The increasing of θ increases the selectivity of the cell for the collection of light at intermediate wavelengths.

ered as favourable work conditions for the cell. At the highest angles ($> 50°$), a portion of light undergoes only one bounce on the pyramids facets (see Fig. 7), with a consequent increase of the overall reflectance. The ARC becomes more selective respect to the wavelength, when the number of bounces on it is reduced, and this could explain the increasing of the slope of the reflectance curve at the extremes of the wavelength range, as shown in Fig. 11.

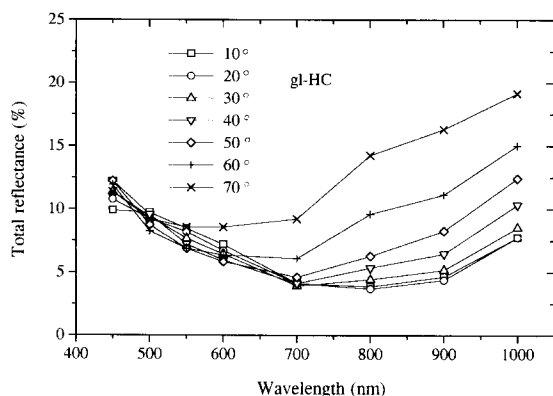Fig. 12 shows the spectral reflectance curves of the gridless HC cell, gl-HC. The behaviour of this cell differs substantially from the gl-PERL one. First of all, the more pronounced reflectance of the HC cell at long wavelengths and low θ values is due to the thinner wafer, which allows a higher reflection from the back metallic contact. The light is increasingly reflected at the increasing angles, particularly at the longest wavelengths. Such a monotonous behaviour, should not depend, as was for the PERL cell, on the variation of the incidence angle of light on the ARC, as that remains mainly unchanged. A possible interpretation of this result is that the inclined incident light crosses the thin region which separates two neighbouring wells, and is reflected at an unfavourable angle at the well of arrival, with a consequent decoupling from the cell. This phenomenon should be enhanced for light with longer wavelength, as an effect of its higher transmittance through the layer separating two adjacent wells, and this is what experimentally found (see Fig. 12). The reflectance at short wavelengths remains quite unchanged by inclining the cell. At particular wavelengths (500–600 nm), the HC cell collects light at high angles even better than at low ones. The larger size of the honeycomb wells (14 μm with respect to the 10 μm pyramids of the PERL cell) could also have affected the reflectance behaviour of the HC cell, but it is not clear in which way. Fig. 13, finally, shows the spectral reflectance curves of the gl-ES cell. The curves move upwards at increasing the
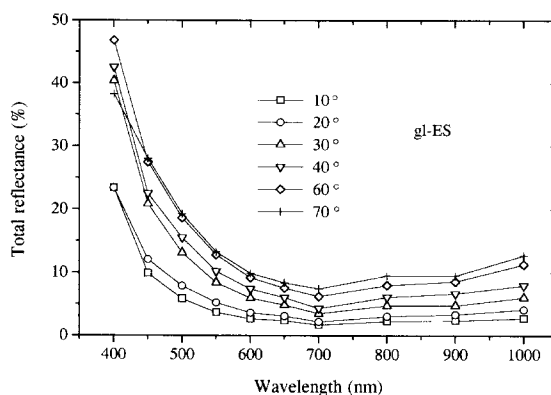

Fig. 12. Filter spectral reflectance, $R_{tot}(\theta,\lambda)$, of the 'gridless' HC (honeycomb) cell, reported at different incidence angles. The optical loss of the cell is particularly evident at long wavelengths. At short wavelengths, the cell reflectance becomes quite insensitive to the incidence angle. At some angles, the optical loss becomes even reduced.

Fig. 13. Filter spectral reflectance, $R_{tot}(\theta,\lambda)$, of the 'gridless' ES (Eurosolare) cell, at different incidence angles. The optical loss increases quite homogeneously on the entire spectrum, at increased incidence angles. At short wavelengths, the reflectance reaches values as high as about 50%.

incidence angle. They show a more homogeneous optical loss over the entire wavelength spectrum, with respect to the other cells. This result could be attributed to the random character of the upright pyramids structure.

5. Summary and conclusions

We have presented the results of reflectance measurements on silicon materials, screen printed and record efficient crystalline silicon solar cells, obtained by using a reflectometer employing a 40 cm diameter integrating sphere. Measurements have been carried out at variable incidence angles and wavelengths of the light beam, by using a He–Ne laser and a QTH lamp, as light sources. The results of all these measurement are very useful for guiding the fabrication and the applications of these solar cells and solar materials.

Particularly interesting, record efficient cells, textured by inverted pyramids (PERL cells), have shown the lowest reflection comparing to any other types of cells tested. As an outstanding result, the reflection maintains low up to an incidence angle as high as 80°. The incident plane parallel to the metal grid gives lower surface reflection at higher incidence angles for the PERL cells. The superior performances of the PERL cell structure, well established both theoretically and experimentally [10,13], are here confirmed relatively to their optical properties, at conditions of changing incidence angle of light. 'Honeycomb' cells, that is cells with a honeycomb structure of hemispherical wells, have shown a slightly higher reflection respect to the PERL cells, particularly at the highest angles of incidence, but a better transmittance relative to the normal incidence up to 60° in the 500–600 nm wavelength range. The screen printed, randomly textured c-Si cells have shown a roughly homogeneous increasing of the spectral reflectance at increasing incidence angles. A model, for considering the reflectance of the grid from that of the cell, has been derived. It has been positively verified by comparing the calculated reflectance of PERL cells with that of 'gridless' PERL cells, specially fabricated for the optical measurements. The model, therefore, can be applied to derive the reflectance of the optically-active area of newly designed solar cells.

Acknowledgements

References

[1] IEC Standards 891 and 1215, Bureau Central de la Commission Electrotechnique Internationale, Genève.

[2] A. Parretta, A. Sarno, L. Vicari, Effects of solar irradiation conditions on the outdoor performance of photovoltaic modules, Opt. Commun. 153 (1998) 153–163.

[3] Patent It. a.n. RM 97A000676, 5 November 1997.

[4] A. Parretta, A. Sarno, H. Yakubu, A Novel Apparatus for the Optical Characterization of Solar Cells and Photovoltaic Modules, Proceedings of the 2nd World Conference and Exhibition on Photovoltaic Solar Energy Conversion, Wien, Austria, 6–10 July 1998, Joint Research Centre, European Commission, 1998, p. 2306.

[5] A. Parretta, A. Sarno, H. Yakubu, Non-destructive optical characterization of photovoltaic modules by an integrating sphere. Part I: Mono-Si modules, Opt. Commun. 161 (1999) 297–309.

[6] J. Zhao, A. Wang, P. Altermatt, M.A. Green, Twenty-four percent efficient silicon solar cells with double layer antireflection coatings and reduced resistance loss, Appl. Phys. Lett. 66 (1995) 3636–3638.

[7] J. Zhao, A. Wang, M.A. Green, F. Ferrazza, 19.8% Efficient 'Honeycomb' textured multicrystalline and 24.4% monocrystalline silicon solar cells, Appl. Phys. Lett. 73 (1998) 1991–1993.

[8] J. Zhao, A. Wang, M.A. Green, 19.8% Efficient Multicrystalline Silicon Solar Cells with 'Honeycomb' Textured Front Surface, Proceedings of the 2nd World Conference and Exhibition on Photovoltaic Solar Energy Conversion, Wien, Austria, 6–10 July 1998, Joint Research Centre, European Commission, 1998, p. 1681.

[9] M.A. Green, Silicon Solar Cells, Advanced Principles and Practices, Centre for Photovoltaic Devices and Systems, UNSW, Sydney, NSW, p. 210.

[10] M.A. Green, Silicon Solar Cells, Advanced Principles and Practices, Centre for Photovoltaic Devices and Systems, UNSW, Sydney, NSW, p. 92.

[11] M.A. Green, J. Zhao, A. Wang, in: J. Shmid, H.A. Ossenbrink, P. Helm, H. Ehmann, E.D. Dunlop (Eds.), Proceedings of the 2nd World Conference and Exhibition on Photovoltaic Solar Energy Conversion, Wien, Austria, 6–10 July 1998, Joint Research Centre, Ispra, 1998, p. 1187.

[12] S.R. Wenham, M.A. Green, M.E. Watt, Applied Photovoltaics, Centre for Photovoltaic Devices and Systems, UNSW, Sydney, NSW, p. 79.

[13] S.R. Wenham, M.A. Green, Prog. Photovoltaics: Res. Appl. 4 (1996) 3–33.

[14] G.E. Jellison Jr., R.F. Wood, Solar Cells 18 (1986) 93–114.